Influence of Reduced Field Strength on Product Ion Formation in High Kinetic Energy Ion Mobility Spectrometry (HiKE-IMS)

Christoph Schaefer*, Maria Allers, Ansgar T. Kirk, Florian Schlottmann, Stefan Zimmermann

Leibniz University Hannover, Institute of Electrical Engineering and Measurement Technology, Department of Sensors and Measurement Technology, Appelstr. 9A, 30167 Hannover, Germany

*Corresponding author: schaefer@geml.uni-hannover.de

Keywords: corona discharge ionization; ionization; APCI; ion mobility spectrometry; high kinetic energy ion mobility spectrometry; HiKE-IMS; IMS

Abstract

Classical ion mobility spectrometers (IMS) operated at ambient pressure, often use atmospheric pressure chemical ionization (APCI) sources to ionize organic compounds. In APCI, reactant ions ionize neutral analyte molecules via gas-phase ion-molecule reactions. The positively charged reactant ions in purified, dry air are H_3O^+, NO^+, and $O_2^{+\bullet}$. However, the hydration of reactant ions in classical IMS operated at ambient pressure renders ionization of certain analytes difficult. In contrast to classical IMS operated at ambient pressure, High Kinetic Energy Ion Mobility Spectrometers (HiKE-IMS) are operated at a decreased pressure of 10 - 40 mbar, allowing operation at high reduced electric field strengths of up to 120 Td. At such high reduced field strengths, ions reach high effective temperatures causing collision-induced cluster dissociation of the hydrated gas-phase ions, allowing ionization of non-polar and low proton affinity analytes. The reactant ion population, consisting of $H_3O^+(H_2O)_n$, $NO^+(H_2O)_m$, and $O_2^{+\bullet}(H_2O)_p$ with an individual abundance that strongly depends on the reduced field strength, differs from the reactant ion population in IMS operated at ambient pressure, which affects the ionization of analyte molecules. In this work, we investigate the influence of reduced field strength on the product ion formation of aromatic hydrocarbons used as model substances. A HiKE-IMS-MS coupling was used to identify the detected ion species. The results show that the analytes form parent cations via charge transfer with $NO^+(H_2O)_m$ and $O_2^{+\bullet}(H_2O)_p$ depending on ionization energy and protonated parent molecules via proton transfer and ligand switching with $H_3O^+(H_2O)_n$ mainly depending on proton affinity.

Introduction

Ion mobility spectrometers (IMS) are widely used in both ion polarities to detect organic compounds, including drugs,[1,2] explosives,[3,4] chemical warfare agents,[5,6] and toxic industrial chemicals (TICs) such as aromatic hydrocarbons[7,8]. An IMS separates different ion species in a drift region based on their ion mobility in a neutral gas under the influence of an electric field. Typically, IMS are equipped with atmospheric pressure chemical ionization (APCI) sources operated at ambient pressure, where reactant ions ionize the analyte molecules via gas-phase reactions in a reaction region. The main advantages of using IMS with APCI sources are their low limits of detection down to the single-digit ppt_V (parts-per-trillion by volume) range in short measurement times of less than one second.[9,10]

However, classical IMS with APCI sources operated at ambient pressure suffer from strong matrix effects and a limited ionization yield for various VOCs. The positively charged reactant ions are hydronium ions H_3O^+, nitrosonium ions NO^+, and oxygen radical ions $O_2^{+\bullet}$. However, in the presence of water molecules, these reactant ions form hydrates. The hydrated NO^+ and hydrated $O_2^{+\bullet}$ react with neutral water molecules to form hydrated hydronium ions, preventing these reactant ions from participating in product ion formation. Consequently, hydrated hydronium ions $H_3O^+(H_2O)_n$ with n = 3

and n = 4 are the most abundant reactant ions at ambient pressure.[10] These hydrated hydronium ions can only ionize analyte molecules via proton transfer if the analytes have a higher proton affinity (PA) than the corresponding water cluster $(H_2O)_{n+1}$. However, since the PA of water clusters increases with increasing cluster size, the hydration of H_3O^+ impairs the ionization of low proton affinity analytes. Furthermore, the formation of large hydrates of H_3O^+ impairs the ionization of non-polar analytes via ligand switching since the reaction rate coefficient of ligand switching seems to decrease with increasing cluster size n of the hydrated hydronium ions.[11–13]

To overcome the limitations of IMS operated at ambient pressure, we introduced the High Kinetic Energy Ion Mobility Spectrometer (HiKE-IMS)[14]. As in classical IMS, analytes are ionized in a reaction region and then separated in a drift region. However, HiKE-IMS are operated at a decreased pressure of 10 – 40 mbar allowing the operation at high reduced electric field strengths E/N of up to 120 Td (1 Td = $1 \cdot 10^{-21}$ Vm²). The reduced electric field strength, which is the ratio of the applied electric field E and the density of neutral molecules N, strongly influences the effective temperature T_{eff} given by eq. 1,[15] which is the average ion-neutral collision energy in the center-of-mass frame of the ions and neutral molecules. In eq. 1, T is the absolute temperature, M is the mass of the neutral molecules, k_B is the Boltzmann constant, K_0 is the reduced ion mobility, N_0 is the Lohschmidt constant, and E/N is the reduced electric field strength.

$$T_{eff} = T + \frac{M}{3k_B}\left[K_0 N_0 \frac{E}{N}\right]^2 \qquad 1$$

Due to the decreased number of collisions at the reduced operating pressure and the decreased reaction times at the high E/N in HiKE-IMS, the ion population is kinetically controlled, in contrast to the thermodynamically controlled ion population in IMS operated at ambient pressure. In addition, in HiKE-IMS, the high effective temperatures cause the hydrates of gas-phase ions to dissociate during collisions. The collision-induced cluster dissociation of $H_3O^+(H_2O)_n$ at high E/N allows the ionization of low proton affinity and non-polar analytes via proton transfer and ligand switching. Furthermore, the collision-induced cluster dissociation of hydrated NO^+ and hydrated $O_2^{+\bullet}$ at high E/N inhibits their conversion to hydrated hydronium ions.[16] Thus, in contrast to IMS operated at ambient pressure, NO^+ and especially $O_2^{+\bullet}$ can participate in product ion formation and ionize analyte molecules via charge transfer even at elevated background water concentrations.

The presence of multiple reactant ion species depending on E/N ionizing analytes on different ionization pathways leads to the formation of multiple product ion species for a single analyte. While the presence of multiple product ions can help to minimize false positives, it also complicates the interpretation of HiKE-IMS spectra. Since the reactant ion population in HiKE-IMS differs from that at ambient pressure and product ion formation thus proceeds via different reaction pathways, detailed studies on the product ion formation in HiKE-IMS are necessary. In a previous work, the product ion formation of acetonitrile, benzene, methanol, and phosphine was investigated.[17] However, there are still several aspects of product ion formation in HiKE-IMS that require further investigation. To use a HiKE-IMS for the detection of VOCs, it is not only necessary to understand which product ions are formed, but especially why and how these product ions are formed. Therefore, it is necessary to investigate which reactant ions are involved in the formation of the individual product ions depending on E/N and on which reaction pathway the product ions are formed. In addition, it is necessary to investigate the reactions of the analytes with the hydrated hydronium ions of different cluster size n and whether the protonation of analytes proceeds via proton transfer or ligand switching. Also, the influence of analyte properties such as proton affinity (PA), ionization energy (IE), and polarity on the proceeding reactions and thus on the formation of the different product ions requires more detailed investigation. The results of this study can also be beneficial for other devices ionizing analytes with the same reactant ions via the same gas-phase ion-molecule reactions, such as selected ion flow tube

mass spectrometers (SIFT-MS)[18,19] or proton transfer reaction mass spectrometers (PTR-MS) when equipped with a switchable reactant ion source.[20,21]

The product ion formation in HiKE-IMS depending on *E*/*N* is studied in this work using aromatic hydrocarbons as model substances. A HiKE-IMS-MS coupling[22] was used to identify the detected ion species. The aromatic hydrocarbons are suitable model substances, as their PA and IE vary over a wide range, allowing investigations of the influence of these quantities on ionization. As the aromatic hydrocarbons can form multiple product ion species in HiKE-IMS[23], studies on their product ion formation can provide more profound insights into different reaction pathways such as charge transfer, proton transfer, and ligand switching. Another reason for aromatic hydrocarbons being suitable model substances is that they do not form fragments in HiKE-IMS, which would further complicate product ion formation. However, an investigation of fragmentation in HiKE-IMS would exceed the scope of this work. In addition, the investigation of the product ion formation at different *E*/*N* allows the investigations on the reactions between the different hydrates of the reactant ions and analyte molecules due to the field-dependent cluster size of the reactant ions.

Ion Formation in HiKE-IMS

The reactant ion formation in HiKE-IMS in positive polarity was investigated in detail in previous work by coupling the HiKE-IMS to a mass spectrometer and is therefore only briefly discussed here.[16,22] In HiKE-IMS, the reaction cascades are initiated by electrons generated in a corona discharge. These electrons initially ionize the main constituents of the sample gas. Therefore, the primary ions in purified air are nitrogen radical ions $N_2^{+\bullet}$, nitrosonium ions NO^+, and oxygen radical ions $O_2^{+\bullet}$. In the presence of trace amounts of water, $N_2^{+\bullet}$ reacts in a reaction cascade to form hydronium ions H_3O^+.[24,25] Consequently, H_3O^+, NO^+, and $O_2^{+\bullet}$ are the main positively charged reactant ions present in HiKE-IMS in purified air. Depending on water concentration, pressure, and effective temperature, the reactant ions can form hydrates according to the association reactions 2 - 4.[26–28]

$$H_3O^+(H_2O)_{n-1} + H_2O \rightleftharpoons H_3O^+(H_2O)_n \quad (2)$$

$$NO^+(H_2O)_{m-1} + H_2O \rightleftharpoons NO^+(H_2O)_m \quad (3)$$

$$O_2^{+\bullet} + H_2O \rightleftharpoons O_2^{+\bullet}(H_2O) \quad (4)$$

However, the hydrates of NO^+ are only stable up to a cluster size of $m \leq 3$, while $O_2^{+\bullet}(H_2O)$ is the only stable hydrate of $O_2^{+\bullet}$. The hydrates $NO^+(H_2O)_3$ and $O_2^{+\bullet}(H_2O)$ react with neutral water molecules to form $H_3O^+(H_2O)_2$ and H_3O^+ according to reactions 5 - 6.[29–33]

$$NO^+(H_2O)_3 + H_2O \rightarrow H_3O^+(H_2O)_2 + HNO_2 \quad (5)$$

$$O_2^{+\bullet}(H_2O) + H_2O \rightarrow H_3O^+ + OH + O_2 \quad (6)$$

At low *E*/*N*, where cluster association dominates over collision-induced cluster dissociation due to the low effective temperature, NO^+ and $O_2^{+\bullet}$ are converted to hydrated hydronium ions by forming unstable hydrates and thus are not involved in product ion formation. As *E*/*N* increases, the effective temperature increases, shifting the equilibrium of reactions 2 - 4 towards smaller clusters by collision-induced cluster dissociation. At high *E*/*N*, the collision-induced cluster dissociation of $NO^+(H_2O)_3$ and $O_2^{+\bullet}(H_2O)$ combined with the decreased residence time of the ions in the reaction region inhibits their conversion to hydrated hydronium ions, allowing $O_2^{+\bullet}$ and NO^+ to participate in product ion formation. Thus, the reduced field strength strongly influences the reactant ion population in HiKE-IMS due to field-dependent collision-induced cluster dissociation.

Since multiple reactant ions with a field-dependent cluster size are present in HiKE-IMS, analytes can be ionized via multiple gas-phase reactions such as proton transfer, ligand switching, and charge transfer. The hydrated hydronium ions can ionize neutral analyte molecules M by transferring a proton

to the molecules forming the protonated parent molecule MH^+ according to reaction 7. Such proton transfer reactions usually proceed at or close to the collisional rate.[34]

$$H_3O^+(H_2O)_n + M \rightarrow MH^+ + (n+1)H_2O \quad (7)$$

The proton affinity (PA) is the negative reaction enthalpy of the proton acceptance reaction.[35] Therefore, the reaction enthalpy $\Delta_r H_{PT}$ of the proton transfer reaction 7 is given by eq. 8.

$$\Delta_r H_{PT} = PA((H_2O)_{n+1}) - PA(M) = \Delta PA \quad (8)$$

The change in Gibbs energy in a proton transfer is given by the difference in gas basicities between the respective neutral water cluster and the neutral analyte molecule M. However, the entropy change in proton transfer can usually be assumed negligible. Thus, the difference in proton affinity is often considered instead. If the analyte's PA exceeds that of the respective water cluster $(H_2O)_{n+1}$, proton transfer will proceed spontaneously.[35] At the low *E*/*N* in IMS operated at ambient pressure, the hydration of H_3O^+ predominates over collision-induced cluster dissociation, shifting the equilibrium of reaction 2 towards larger clusters $H_3O^+(H_2O)_3$ with $PA((H_2O)_4)$ = 919 kJ/mol and $H_3O^+(H_2O)_4$ with $PA((H_2O)_5)$ = 926 kJ/mol at a background water concentration of 50 ppm_V having a higher PA than H_2O (691 kJ/mol).[10,36–39] Thus, the ionization of low proton affinity analytes via proton transfer is impaired. In contrast, at the high *E*/*N* in HiKE-IMS, H_3O^+ is formed by collision-induced cluster dissociation. Since H_2O has a lower PA than most organic compounds of 691 kJ/mol, protonation of low proton affinity analytes is possible in HiKE-IMS.

Besides proton transfer, $H_3O^+(H_2O)_n$ can ionize analyte molecules in ligand switching reactions forming hydrates of the protonated parent molecule according to reaction 9. The reaction rate coefficient of ligand switching seems to increase with increasing polarizability and permanent dipole moment of the analyte molecules.[11,28,40] In contrast, the reaction rate coefficient seems to decrease with increasing cluster size *n*.[11–13]

$$H_3O^+(H_2O)_n + M \rightarrow MH^+(H_2O)_k + (n+1-k)H_2O \quad (9)$$

According to Hess' law, the reaction enthalpy $\Delta_r H_{LS}$ of ligand switching is determined by dividing reaction 9 into a sequence of proton acceptance and proton donation reactions, as well as in hydration and dehydration reactions and forming the sum of the enthalpy changes of the individual reactions.[41] As discussed above, the reaction enthalpy of the proton acceptance and proton donation is given by the PA of the respective water cluster and the analyte molecule. The reaction enthalpy of the hydration and dehydration is given by the bond energy between the ligand and the bound molecule E_{bond}. In this case, the bound molecule is H_2O and thus E_{bond} is the hydration energy. Consequently, the reaction enthalpy $\Delta_r H_{LS}$ of ligand switching is given by eqs. 10 and 11.[42] Since the PA is a positive quantity and the hydration energy is a negative quantity, ligand switching is facilitated by a high PA of the analyte molecules or by a strong bond between MH^+ and H_2O. Note that the reaction enthalpy of ligand switching for analytes with $H_3O^+(H_2O)_n$ only depends on the PA of the water monomer (691 kJ/mol) whereas the reaction enthalpy of proton transfer with $H_3O^+(H_2O)_n$ depends on the PA of the respective water cluster $(H_2O)_{n+1}$. Since the PA of the water clusters increases with cluster size *n*, the term ΔPA in eq. 11 is more exothermic for ligand switching than for proton transfer with the same hydrated hydronium ions. Thus, depending on the difference in hydration energy ΔE_{hyd} between the protonated parent molecule of the analyte and the hydronium ion, ligand switching with a given hydrated hydronium ion may be exothermic, although proton transfer with the same reactant ion is endothermic.

$$\Delta_r H_{LS} = \sum_{j=1}^{k} E_{Hyd}\left(MH^+(H_2O)_{j-1,j}\right) - \sum_{i=1}^{n} E_{Hyd}\left(H_3O^+(H_2O)_{i-1,i}\right) + PA(H_2O) - PA(M) \quad (10)$$

$$\Delta_r H_{LS} = \Delta E_{Hyd} + \Delta PA \quad (11)$$

Furthermore, both NO^+ and $O_2^{+\bullet}$ can ionize analyte molecules via charge transfer forming the parent radical cations $M^{+\bullet}$ according to reactions 12 - 13. Usually, charge transfer proceeds at or close to the collisional rates. If the analyte molecule has a lower ionization energy (IE) than the reactant ions with IE(NO) = 9.26 eV and IE(O_2) = 12.07 eV,[43] charge transfer can proceed spontaneously.[35] However, the high ionization energy of O_2 compared to that of many volatile organic compounds can result in significant excess energy in the reaction, causing fragmentation of the product ions.[44]

$$NO^+ + M \rightarrow M^{+\bullet} + NO \quad (12)$$

$$O_2^{+\bullet} + M \rightarrow M^{+\bullet} + O_2 \quad (13)$$

The hydrated NO^+ can also ionize analytes via charge transfer. The reaction enthalpy $\Delta_r H_{CT}$ is determined using Hess' law and given by eq. 14. Since the hydration energy of NO^+ and its hydrates is negative, the reaction enthalpy of charge transfer with the hydrated NO^+ is more endothermic than the charge transfer with NO^+. Thus, hydration of NO^+ can inhibit the ionization of analytes via charge transfer.

$$\Delta_r H_{CT} = IE(M) - IE(NO) - \sum_{i=1}^{n} E_{Hyd}(NO^+(H_2O)_{i-1,i}) \quad (14)$$

Smith et al. have shown that the hydrated NO^+ can ionize analyte molecules via ligand switching according to reaction 15 forming hydrated adducts $M{\cdot}NO^+$ if the NO^+-M bond energy exceeds the NO^+-H_2O bond energy.[45] $NO^+(H_2O)$ seems to ionize analytes via ligand switching only when charge transfer is endothermic. In HiKE-IMS, due to the high *E*/*N*, the adducts can fragment and form NO^+ or the radical cation $M^{+\bullet}$, if the charge of NO^+ is transferred to the analyte molecule.

$$NO^+(H_2O)_m + M \rightarrow M \cdot NO^+(H_2O)_k + (m-k)H_2O \quad (15)$$

Gas-phase ion-molecule reactions of aromatic hydrocarbons

The gas-phase reactions of aromatic hydrocarbons with H_3O^+, NO^+, and $O_2^{+\bullet}$ have already been investigated in selected ion flow tube (SIFT) studies,[46] showing that H_3O^+ reacts via proton transfer forming the protonated parent molecule MH^+. NO^+ ionizes the aromatic hydrocarbons via non-dissociative charge transfer forming the parent radical cation $M^{+\bullet}$ and reacts with benzene via adduct formation. The large difference in IE between O_2 and the aromatic hydrocarbons leads to partially dissociative charge transfer for reactions with $O_2^{+\bullet}$. Also, the influence of temperature on reactions of $H_3O^+(H_2O)_n$ with n = 0 and n = 1, NO^+, and $O_2^{+\bullet}$, was investigated using SIFT and flowing afterglow (FA) techniques at various absolute temperatures.[47–49] At low temperatures, the protonated parent molecule, and the parent radical cation are the most abundant product ion species. However, the excitation of internal energy states and high rovibrational energies at high temperatures opens dissociative proton transfer and dissociative charge transfer channels.

Experimental

For all experiments, we use the same HiKE-IMS as described in detail in an earlier publication.[50] Table 1 summarizes the most relevant operating parameters of the HiKE-IMS. The reduced field strength in both the drift and reaction region can be increased independently up to 120 Td. The reduced reaction field strength E_{RT}/N affects the reactant ion formation and the product ion formation in the reaction region. The reduced drift field E_{DT}/N strength influences the separation in the drift region due to field-dependent ion mobilities. However, E_{DT}/N can also affect the ion population due to field-dependent cluster association, cluster dissociation, and fragmentation inside the drift region. A HiKE-IMS-MS coupling[22] was used to identify the detected ion species.

Table 1. Operating parameters of the HiKE-IMS

Parameter	Value
reaction region length	77 mm
drift region length	306 mm
drift region diameter	21 mm
corona voltage	1300 V
reaction region voltage	0.5 - 5 kV
reduced reaction field, E_{RT}/N	10 - 120 Td
drift region voltage	20 kV
reduced drift field, E_{DT}/N	120 Td
injection time	1 µs
drift gas flow	19 ml_s/min
sample gas flow	19 ml_s/min
operating pressure	14.3 mbar
operating temperature	45 °C
dew point of sample and drift gas	-14.3°C

All chemicals were purchased from Sigma-Aldrich Germany with a purity of > 99 %. The samples were introduced using a permeation oven (Vici, Dynacalibrator Model 150) and homemade permeation tubes. Drift and sample gas are transferred into the HiKE-IMS via capillaries with 250 µm inner diameter. The capillary lengths were adjusted to provide gas flow rates of 19 ml_s/min (milliliter standard per minute, mass flow at reference conditions 20 °C and 1013.25 hPa). A zero air generator (JAG, JAGZAG600S) combined with a pressure swing absorber (PureGas, CAS1) in series with an additional moisture trap (Supelco, Molecular Sieve 5A Moisture Trap, 23991) and an activated carbon filter (Supelco, Supelcarb® HC Hydrocarbon Trap, 24564) supplies purified air containing < 1 ppm_V of water as drift gas. The water concentration in the sample and drift gas is set to 0.2 $\%_V$ by mixing the provided purified air containing < 1 ppm_V of water with purified air passed through a water container. Dew point sensors (Michell Instruments, Easidew Transmitter) measure the resulting water concentration of both sample and drift gas.

Kinetic Model for Computing the Reactant Ion Population in HiKE-IMS

The reactant ion population in HiKE-IMS depending on E_{RT}/N is also computed using the simple kinetic model introduced in previous work.[16] This kinetic model includes bimolecular charge transfer reactions, proton transfer reactions, cluster association reactions, and cluster dissociation reactions, including their corresponding reaction rate coefficients known from the literature. The rate coefficient of collision-induced cluster dissociation is estimated from the rate coefficient of the cluster association reaction, its molar standard reaction enthalpy, and its molar standard reaction entropy using van't Hoff equations[51] and the field-dependent effective temperature T_{eff}, which can be calculated using the Wannier equation according to eq. 1.

Results and Discussion

In the following, product ion formation in HiKE-IMS depending on E_{RT}/N will be examined in more detail. In particular, it is investigated which product ions are formed, how the properties of the analytes affect ionization, and which reactant ions are involved in product ion formation. For such studies, the reactant ion population depending on E_{RT}/N needs to be investigated first.

The formation of positively charged reactant ions in HiKE-IMS depending on E_{RT}/N has been investigated in detail in previous publications.[16,17,22] Therefore, the reactant ion population is studied in this work only in sufficient detail to understand product ion formation. To this end, we recorded HiKE-IMS spectra at a constant background water concentration of 0.2 $\%_V$ inside the reaction region

and various reduced reaction field strengths of 10 - 120 Td. The reduced drift field strength is set to 120 Td in all experiments to mitigate changes in the ion population within the drift region. At such E_{DT}/N, the collision-induced cluster dissociation of $O_2^{+\bullet}(H_2O)$ and $NO^+(H_2O)_3$ inhibits their conversion to hydrated hydronium ions inside the drift region as much as possible. First, the measurement is conducted without injecting analytes to investigate reactant ion formation. Subsequently, the same measurements are conducted with the injection of analytes with a volume fraction of 0.5 ppm_V in the reaction region of the HiKE-IMS.

Influence of Reduced Reaction Field Strength on Reactant Ion Formation

Figure 1 a) shows HiKE-IMS spectra without analyte injection in purified air at different E_{RT}/N. The ion current at the end of a reaction region of an IMS with corona discharge ionization source increases quadratically with increasing E_{RT}/N, resulting in increasing peak amplitudes in the ion mobility spectrum with increasing E_{RT}/N.[52] For this reason, instead of the varying absolute intensity, the relative abundance of the ion species, which is the fraction of an ion species in the HiKE-IMS spectrum, is used to investigate the ion population in HiKE-IMS depending on E_{RT}/N. The relative abundance of an individual ion species is determined by dividing the peak area of an ion by the integral of the HiKE-IMS spectrum corresponding to the ratio of the charge underlying the peak of the ion species and the total charge underlying the IMS spectrum.

The relative abundances of the individual reactant ion species are shown in Figure 1 b). It can be seen that hydrated hydronium ions are the only detected reactant ions up to a reduced reaction field strength of 40 Td. As expected, NO^+ and $O_2^{+\bullet}$ are converted to hydrated hydronium ions at low E_{RT}/N, since they form hydrates that subsequently react with water molecules. Above about 40 Td, the conversion of NO^+ is inhibited as collision-induced cluster dissociation becomes more significant and, also, the reaction time decreases at high E_{RT}/N. Above about 60 Td, the relative abundance of NO^+ remains constant, indicating that the conversion is completely inhibited. Note that the measurement agrees well with the relative abundance of the reactant ions simulated using the simple kinetic model.

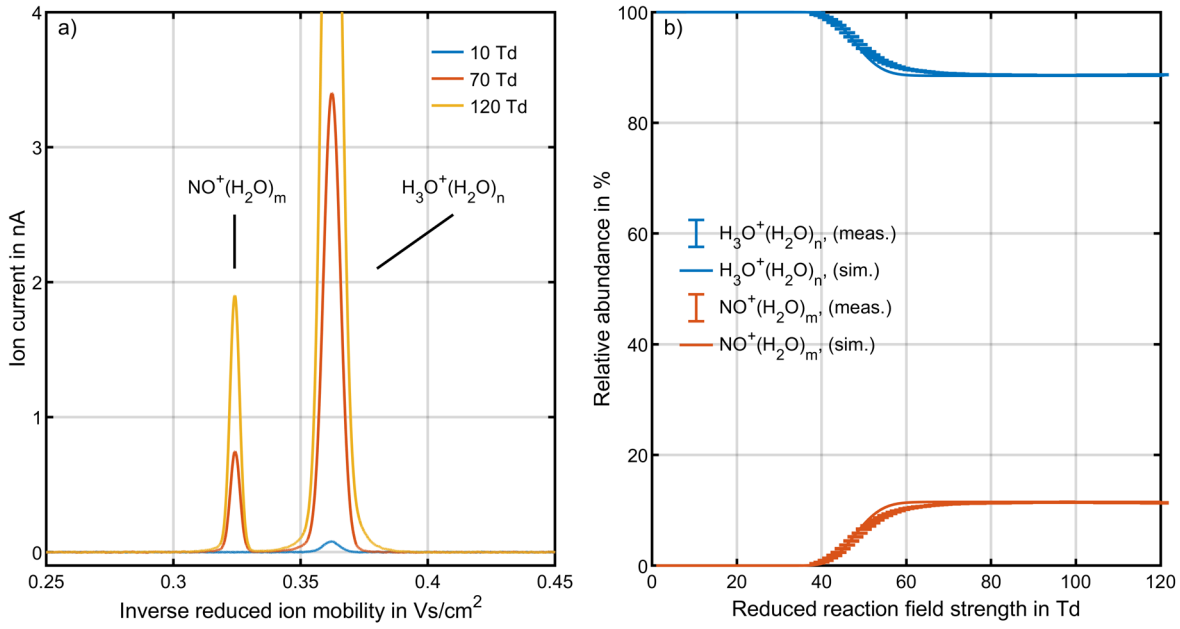

Figure 1. Reactant ion population in HiKE-IMS in purified air depending on reduced reaction field strength at a water concentration inside the reaction region of 0.2 $\%_V$. a) Positive HiKE-IMS spectra of the reactant ions at different reduced reaction field strengths. b) Comparison of measured (meas.) and simulated (sim.) relative abundances of the reactant ions. All simulations were carried out using the kinetic model described in previous work.[16] Table 1 summarizes all other operational parameters. The error bars for the measured relative abundances in b) represent the standard deviation of three individual measurements without analyte injection.

In contrast to NO^+, $O_2^{+\bullet}$ is not detected even at the maximum reduced reaction field strength of 120 Td. Nevertheless, as shown in a previous publication,[17] $O_2^{+\bullet}$ may still be present in parts of the reaction region, especially near the corona needle. Thus, $O_2^{+\bullet}$ may participate in product ion formation even though it is converted to H_3O^+ later and not detected in the HiKE-IMS spectrum.

After injecting the ions generated in the reaction region into the drift region, the equilibrium of the association reactions 2 and 3 shifts depending on the reduced drift field strength and water concentration inside the drift region. Due to the high E_{DT}/N of 120 Td used in this work, the hydrates formed in the reaction region quickly dissociate within the drift region.[53] As a result, the ions travel through the drift region at the same drift velocity regardless of their cluster size within the reaction region. For this reason, the cluster size of the reactant ions within the reaction region, significantly affecting the ionization of analyte molecules, can only be investigated by kinetic modeling.

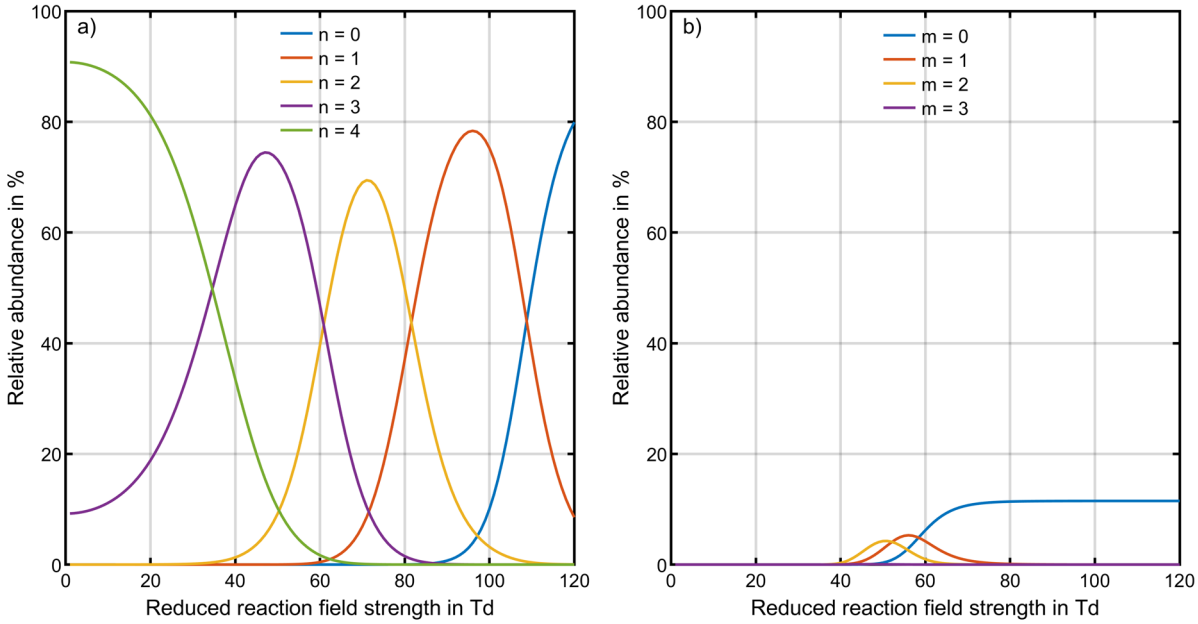

Figure 2. Simulated relative abundances of the hydrates of H_3O^+ and NO^+ in purified air depending on reduced reaction field strength at a water concentration inside the reaction region of 0.2 $\%_v$. a) Simulated relative abundances of $H_3O^+(H_2O)_n$ with different cluster sizes *n*. b) Simulated relative abundances of $NO^+(H_2O)_m$ with different cluster sizes *m*. All simulations were carried out using the kinetic model described in previous work.[16]

Figure 2 shows the simulated relative abundances of the hydrates of H_3O^+ and NO^+ depending on E_{RT}/N. At low E_{RT}/N of about 1 – 10 Td, the hydronium ions form clusters with four water molecules. As E_{RT}/N increases, the cluster size decreases due to collision-induced cluster dissociation. While the monohydrate of H_3O^+ becomes present above 60 Td, H_3O^+ forms above about 90 Td. At 120 Td, the hydration of H_3O^+ is almost completely prevented. The hydrates of NO^+ also dissociate with increasing E_{RT}/N. At 50 Td, mainly the monohydrate and dihydrate of NO^+ are present, while above 70 Td, almost only NO^+ is present. The dependence of the reactant ions' cluster size on E_{RT}/N provides an important insight into product ion formation in HiKE-IMS. The changes in PA and IE of the reactant ions due to collision-induced cluster dissociation benefit the ionization of analytes. The PA of $(H_2O)_{n+1}$ decreases with decreasing cluster size and the IE of $NO^+(H_2O)_m$ increases with decreasing cluster size, both allowing the ionization of a broader spectrum of analytes.

Influence of Reduced Reaction Field Strength on Product Ion Formation

The ionization via charge transfer and proton transfer according to reactions 7, 12 and 13 can be considered as pseudo-first-order regarding the ion species since the neutral reactants are present in vast excess.[54] As derived in reference [28], eq. 16 describes the dependence of the charge density of the

product ions ρ_{M^+} on the reaction rate coefficient *k*, the product of the volume fraction of the analyte molecules ϕ_M and the neutral gas density *N*, the reaction time Δt, and the charge density of the reactant ions involved in ionization ρ_{R^+}.

$$\rho_{M^+} = \rho_{R^+}(1 - \exp(-k[M]\Delta t)) \approx k\phi_M N\Delta t\rho_{R^+} \quad 16$$

Often it is more convenient to consider currents instead of charge densities. With the current *I* as the product of charge density and drift velocity of an ion species and the cross-sectional area of the detector, eq. 17 is obtained, where the cross-sectional area is eliminated. Instead of the ratio of drift velocities, the ratio of reduced ion mobilities can be used.

$$I_{M^+} = k\phi_M N\Delta t I_{R^+} \frac{v_{M^+}}{v_{R^+}} = k\phi_M N\Delta t I_{R^+} \frac{K_{0,M^+}}{K_{0,R^+}} \quad 17$$

In eq. 17, the reaction rate coefficient with a given reactant ion species *k*, the volume fraction of the neutral molecules ϕ_M, and the neutral gas density *N* can be assumed constant. Thus, the current of the product ions I_{M^+} depends on the reaction time Δt, the current of the reactant ions involved in ionization I_{R^+}, and the ratio of reduced ion mobilities of product ions and reactant ions. The current of reactant ions involved in ionization strongly depends on E_{RT}/N due to the field-dependent collision-induced cluster dissociation and conversion of NO^+ and $O_2^{+\bullet}$ to hydrated hydronium ions. The reaction time is the time required for the ions to travel through the reaction region and is thus inversely proportional to E_{RT}/N. Furthermore, the ratio of reduced ion mobilities slightly depends on E_{RT}/N due to different field-dependencies of the reduced ion mobilities of the product ions and the reactant ions. However, the influence of changes in the ratio of reduced ion mobilities on I_{M^+} are neglected here, since the changes in Δt and I_{R^+} have a more significant influence on I_{M^+}.

If an analyte already reacts with the reactant ions present at a given reduced field strength, increasing E_{RT}/N does not increase the relative abundance of reactant ions involved in ionization. Thus, if the reaction rate coefficient *k* does not significantly increase by cluster dissociation, the relative abundance of a product ion species decreases with increasing E_{RT}/N due to the decreasing reaction time. Vice versa, an increase in the relative abundance of a product ion species with increasing E_{RT}/N indicates that the relative abundance of reactant ions involved in ionization increases, compensating for the decreasing reaction time. The proportionality between the current of product ions and the current of the reactant ions involved in ionization allows an investigation of the reactant ions involved in the formation of a specific product ion species.

Table 2 summarizes the aromatic hydrocarbons investigated in this work and the quantities relevant for ionization, such as PA, IE, permanent dipole moment, and polarizability. Tables S1 and S2 in the Supporting Information summarize the reaction enthalpies for proton transfer, ligand switching, and charge transfer with the different reactant ions. The entropy change in gas-phase reactions usually can be assumed negligible. For this reason, the change in Gibbs energy is approximately equal to the reaction enthalpy, allowing an evaluation if a reaction can run spontaneously based on the reaction enthalpy. Since most of the investigated aromatic hydrocarbons have a PA between that of the water monomer (691 kJ/mol)[43] and the water dimer (833 kJ/mol)[39], proton transfer is exothermic only with H_3O^+, except for 1,3,5-TMB, where proton transfer with $H_3O^+(H_2O)$ is also exothermic. In addition, ligand switching between the hydrated hydronium ions and benzene is endothermic due to the low hydration energy of MH^+ of benzene. Unfortunately, the hydration energy of the protonated parent molecules of the other aromatic hydrocarbons is unknown, making the accurate calculation of the reaction enthalpy of ligand switching impossible. As discussed by Lau et al.,[55] the hydration of ions with delocalized charges such as benzene is a weak interaction. However, the substituted benzenes have localized charges at the substituent, enhancing the bonding of water molecules. Thus, they should have a higher hydration energy than benzene. Since the substituted benzenes, except for

chlorobenzene and fluorobenzene, also have a significantly higher PA than benzene, ligand switching should be more exothermic for the substituted benzenes than for benzene.

In addition, charge transfer with NO^+ and $O_2^{+\bullet}$ is exothermic for all investigated aromatic hydrocarbons, since they have a lower IE than NO (9.26 eV) and O_2 (12.07 eV).[43] As the reaction enthalpy of charge transfer with the monohydrate of NO^+ is more endothermic by the hydration energy of NO^+, the reaction is exothermic only for p-xylene and the trimethylbenzenes. Consequently, charge transfer with the dihydrate of NO^+ is endothermic for all analytes.

Table 2. Gas-phase ion energetics data including proton affinities (PA) in kJ/mol and ionization energies (IE) in eV for the investigated substances and the neutral precursors of the reactant ions, taken from the NIST Chemistry WebBook.[43] [a] The PA of neutral water clusters $(H_2O)_n$ were taken from reference [39]. [b] A calculation of the PA of 1,2,3-trimethylbenzene and 1,2,4-trimethylbenzene is given by reference [56]. The permanent dipole moments μ_D in debye, D, and the polarizability α in units of 10^{-24} cm^3, are taken from the NIST ***C**omputational **C**hemistry **C**omparison and **B**enchmark **D**ata**B**ase*.[57] [c] Estimations of the permanent dipole moments and polarizabilities of the remaining substances are taken from reference [46].

Compound	PA in kJ/mol	IE in eV	μ_D in D	α in Å^3
H_2O	691	12.62	1.86	1.5
$(H_2O)_2$	833[a]			
$(H_2O)_3$	889[a]			
$(H_2O)_4$	919[a]			
$(H_2O)_5$	926[a]			
oxygen	421	12.07	0	1.56
nitric oxide	531.8	9.26	0.159	1.7
benzene	750.4	9.24	0	9.96
chlorobenzene	753.1	9.07	1.69	11.86
fluorobenzene	755.9	9.20	1.6	10.2
toluene	784	8.83	0.332	11.86
o-xylene	796	8.56	0.62	14.9
m-xylene	812.1	8.55	0.3±0.2[c]	14.9
p-xylene	794.4	8.44	0	14.26
1,2,3-trimethylbenzene (1,2,3-TMB)	815.8[b]	8.42	0.6±0.2[c]	16±0.5[c]
1,2,4-trimethylbenzene (1,2,4-TMB)	817.6[b]	8.27	0.4±0.2[c]	16±0.5[c]
1,3,5-trimethylbenzene (1,3,5-TMB)	836.2	8.40	0	16±0.5[c]

Figure 3 shows the HiKE-IMS spectra and corresponding HiKE-IMS-MS spectra recorded in the selected-mobility mode of the product ion peaks of 1,2,3-trimethylbenzene as an example. The Supporting Information contains the HiKE-IMS spectra and HiKE-IMS-MS spectra of the remaining analytes. While no product ions are detected at low E_{RT}/N, two product ion peaks can be detected for all analytes at high E_{RT}/N, as shown for 1,2,3-TMB in Figure 3. Using the HiKE-IMS-MS spectra, the product ion species are identified as parent radical cation $M^{+\bullet}$ and protonated parent molecule MH^+, agreeing well with expectations.

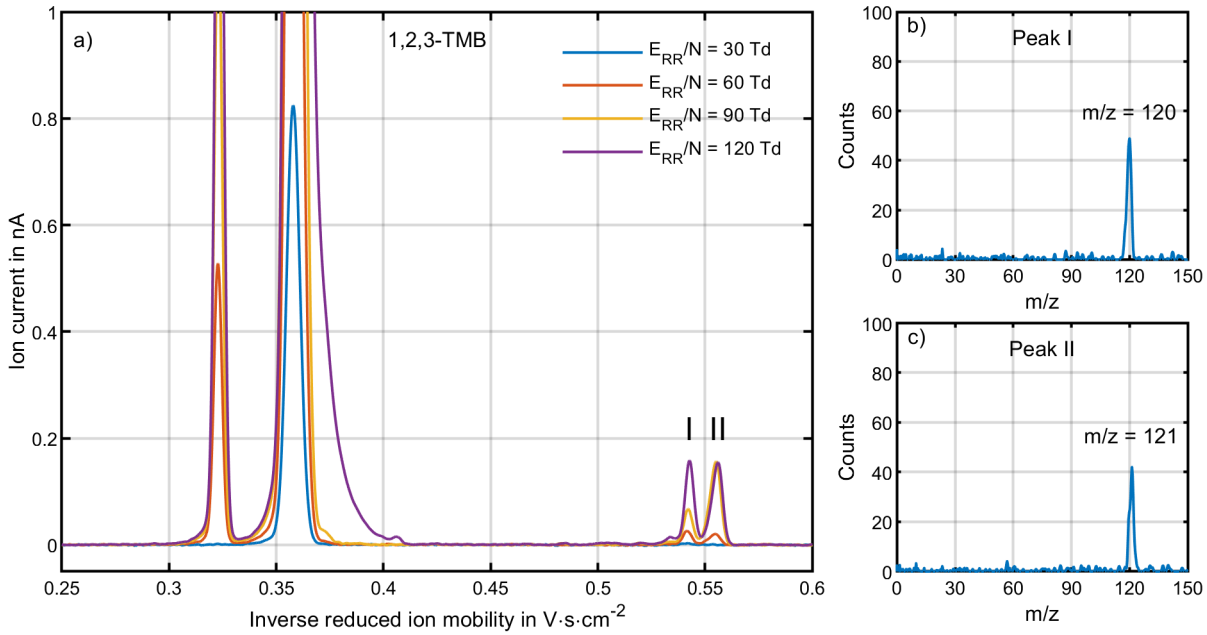

Figure 3. Product ion population of 1,2,3-TMB with a volume fraction of 0.5 ppm_V in HiKE-IMS in purified air at a water concentration inside the reaction region of 0.2 %V. a) Positive HiKE-IMS spectra of 1,2,3-TMB at different reduced reaction field strengths. b) HiKE-IMS-MS spectrum of peak I in the ion mobility spectrum at E_{RT}/N = 120 Td. c) HiKE-IMS-MS spectrum of peak II in the ion mobility spectrum at E_{RT}/N = 120 Td. Table 1 summarizes all other operational parameters.

Figure 4 shows the relative abundances of the parent radical cations and the protonated parent molecules of the aromatic hydrocarbons depending on E_{RT}/N. It can be seen that the relative abundance of $M^{+\bullet}$ shows the same qualitative dependence on E_{RT}/N for all investigated compounds. Above 20 Td, the parent radical cation of the aromatic hydrocarbons can be detected. At such reduced field strength, neither $NO^+(H_2O)_m$ nor $O_2^{+\bullet}$ can be detected. $NO^+(H_2O)_m$ is not detected until a higher E_{RT}/N of about 40 Td. However, at 20 Td, $NO^+(H_2O)_m$ is possibly already present in significant amounts in parts of the reaction region near the corona needle and can thus ionize the analytes via charge transfer, but is converted to hydrated hydronium ions later when traveling through the reaction region. Above 40 Td, the conversion of NO^+ is inhibited to such an extent that a significant amount of the ions reaches the detector. Further increasing E_{RT}/N no longer increases the amount of NO^+ involved in ionization, and the relative abundance of $M^{+\bullet}$ remains constant at reduced reaction field strengths of 40 - 80 Td. Above E_{RT}/N = 80 Td, the relative abundance increases again. Thus, according to eq. 17, the relative abundance of reactant ions involved in ionization increases. At such E_{RT}/N, $O_2^{+\bullet}$ can be present in significant amounts in parts of the reaction region, ionizing the analytes via charge transfer.[17]

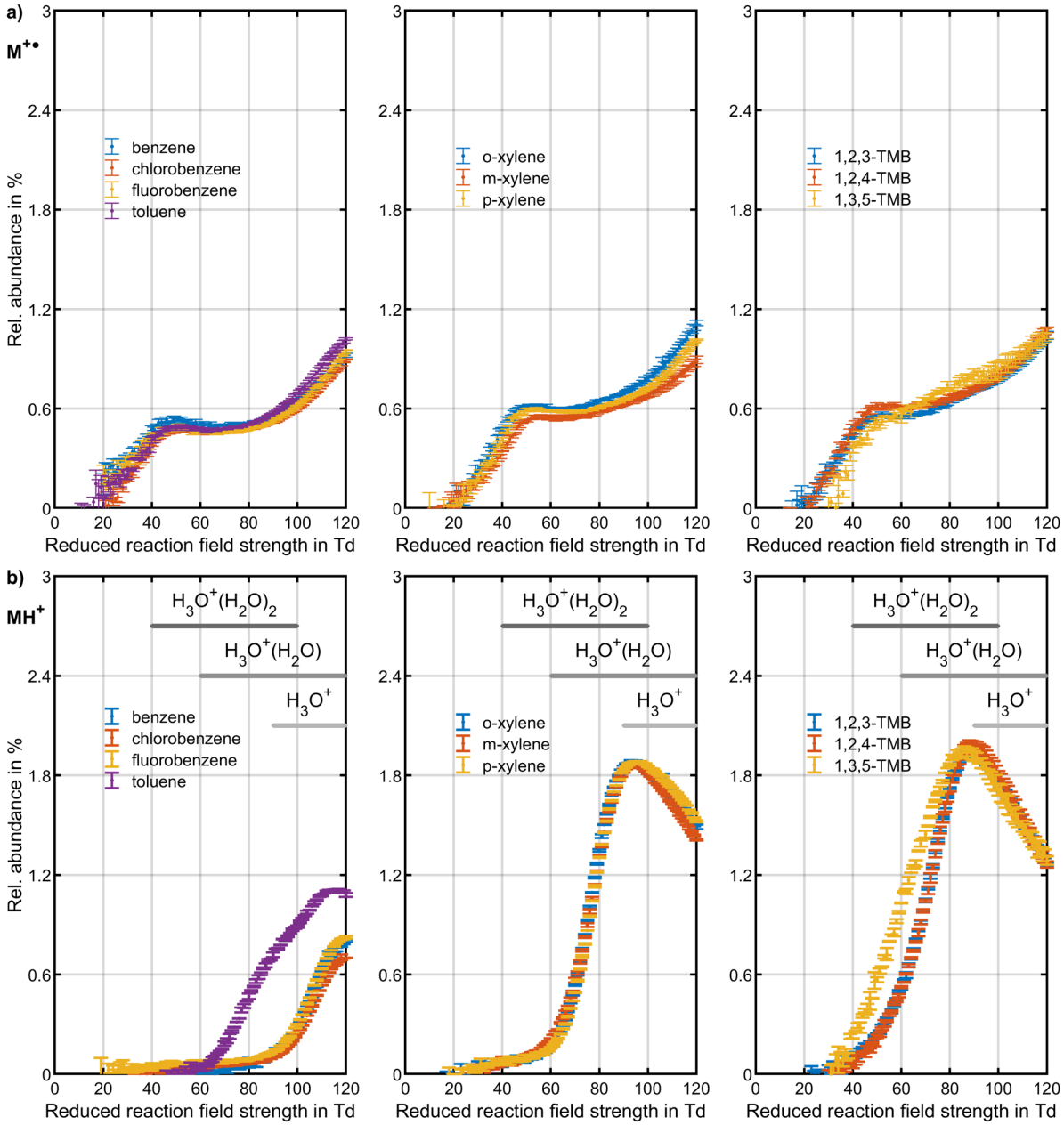

Figure 4. Product ion population of several aromatic hydrocarbons in HiKE-IMS in purified air depending on the reduced reaction field strength at a water concentration inside the reaction region of 0.2 $\%_V$. a) Measured relative abundances of the parent cations $M^{+\bullet}$. b) Measured relative abundances of the protonated parent molecules MH^+. The horizontal lines indicate the reduced reaction field strengths where the relevant hydrates of H_3O^+ are present. The volume fraction of the analyte in the sample gas is 0.5 ppm_V for all substances. Table 1 summarizes all other operational parameters. The error bars represent the standard deviation of three individual measurements of the same sample. Note that the two product ion peaks of 1,3,5-TMB could not be baseline separated.

Unlike the formation of the parent radical cation, the formation of the protonated parent molecules shows different behavior for the different aromatic hydrocarbons. Figure 4 shows that the protonated parent molecules are not detected at low E_{RT}/N but are only formed above a certain reduced field strength that is different for the different analytes. The protonated parent molecules are formed and detected only if sufficiently small clusters of H_3O^+ are formed by collision-induced cluster dissociation, and ligand switching or proton transfer becomes exergonic.

Benzene, chlorobenzene, and fluorobenzene form MH^+ in significant amounts only above about 90 Td, where the hydrated hydronium ions dissociate to H_3O^+. Thus, these compounds seem only reacting with H_3O^+ via proton transfer. In contrast, toluene and the xylenes already form the protonated parent

molecules at about 60 Td, where the monohydrate of H_3O^+ becomes abundant. Presumably, the protonated parent molecules are formed via ligand switching since proton transfer with the monohydrate is endothermic. As explained above, if the relative abundance of reactant ions involved in ionization is constant, the relative abundance of a product ion species should decrease at high E_{RT}/N due to the decreasing reaction time. While this is correct for the xylenes at E_{RT}/N above 90 Td, the relative abundance of toluene increases up to a reduced field strength of about 110 Td. Furthermore, the relative abundance of toluene has significantly smaller values between 60 – 90 Td than that of the xylenes, indicating that ligand switching between toluene and $H_3O^+(H_2O)$ is less efficient than ligand switching between the xylenes and $H_3O^+(H_2O)$. Thus, the relative abundance of MH^+ of toluene possibly increases up to about 110 Td, since the reaction rate coefficient for proton transfer with H_3O^+ is significantly higher than that for ligand switching with $H_3O^+(H_2O)$, compensating for the decreasing reaction time. The trimethylbenzenes already form the protonated parent molecules at about 40 Td and therefore seem to also react with the dihydrate of H_3O^+ via ligand switching. However, the relative abundance increases more rapidly above 60 Td, where the hydrated hydronium ions dissociate to the monohydrate, indicating that the reaction with the monohydrate of H_3O^+ proceeds with a higher reaction rate coefficient. Due to similar ion mobilities, the two product ion peaks of 1,3,5-TMB were not baseline resolved in the HiKE-IMS spectrum, complicating the determination of the peak integrals. This could explain why the dependence of the relative abundance of MH^+ of 1,3,5-TMB slightly differs from that of its isomers. However, Figure 4 and the HiKE-IMS spectra in the Supporting Information show that 1,3,5-TMB seems to form the protonated parent molecule at lower E_{RT}/N than the other aromatic hydrocarbons of about 40 Td.

The formation of the protonated parent molecules provides two main findings. Benzene, chlorobenzene, and fluorobenzene form the protonated monomer at the same reduced reaction field strength and therefore react with the same reactant ion despite having significantly different permanent dipole moments and polarizabilities. The same applies to the xylenes and the trimethylbenzenes. Contrary to expectations, the aromatic hydrocarbons with higher dipole moment and polarizability but similar PA do not react with larger hydrates of H_3O^+ via ligand switching. Possibly, the difference in dipole moment and polarizability are too small to compensate for the low hydration energy caused by the delocalized electrons, causing the reaction enthalpy for ligand switching with larger hydrates to remain endothermic. For a proper calculation of the reaction enthalpy of ligand switching $\Delta_r H_{LS}$, the hydration energy of the protonated parent molecules would be required.

Another finding is that the analytes with higher PA form the protonated parent molecules at lower E_{RT}/N and therefore react with larger hydrates of H_3O^+, presumably via ligand switching, since proton transfer with the hydrates of H_3O^+ is still endergonic in most cases. This finding agrees with expectations since the reaction enthalpy of ligand switching should depend on the analytes' PA. A large difference in PA between the analytes and the water monomer can compensate for the low hydration energy of the aromatic hydrocarbons, making ligand switching with larger hydrates of H_3O^+ exothermic. In addition, analytes having a larger number of functional groups, including the methyl group, seem to react with larger hydrates of H_3O^+. For example, p-xylene, 1,2,3-TMB, and 1,2,4-TMB have a similar PA, but the trimethylbenzenes form the protonated parent molecules at lower E_{RT}/N and thus react with larger hydrates of H_3O^+ than p-xylene. Besides the obvious correlation that the analytes having a higher number of functional groups in most cases have a higher PA, the probability that ligand switching occurs in a collision could depend on the number of functional groups. Possibly, the reaction can only proceed if the functional group and the reactant ion are in a particular orientation during a collision. In this case, the probability of the reactant ion and molecule being in the proper orientation at a collision, and thus the probability for the reaction to proceed, would increase as the number of functional groups increases.

Conclusion

In this work, we investigated the product ion formation of aromatic hydrocarbons used as model substances depending on reduced field strength. The cluster dissociation of reactant ions at the high reduced field strengths in HiKE-IMS allows the ionization of the aromatic hydrocarbons that are difficult to ionize at ambient pressure. On the one hand, depending on proton affinity, the analytes form the protonated parent molecules via proton transfer and ligand switching with $H_3O^+(H_2O)_n$. A higher number of functional groups seems to favor ligand switching. More detailed information on the hydration energy of the protonated parent molecules is required for the proper calculation of the reaction enthalpy for ligand switching. On the other hand, the analytes form the parent radical cation via charge transfer with NO^+ and $O_2^{+\bullet}$ depending on ionization energy.

Thus, product ion formation in HiKE-IMS differs from that at ambient pressure and can be quite complex. While the complexity can complicate the interpretation of HiKE-IMS spectra, the presence of multiple product ion species can also help to minimize false positives. Moreover, a switchable ion source providing only a single reactant ion species could facilitate the interpretation of HiKE-IMS spectra by reducing the number of simultaneous ionization pathways and thus the number of formed product ions. Furthermore, this ion source would allow the separate investigation of the reactions of the individual reactant ion species.

Supporting Information

Reaction enthalpies for the proton transfer and ligand switching; reaction enthalpies for charge transfer; determined reduced ion mobilities of the product ion peaks; HiKE-IMS spectra and HiKE-IMS-MS spectra for all investigated substances

Author Information

Corresponding Author

*Fax: +49 511 762 3917
E-mail: schaefer@geml.uni-hannover.de

Author Contributions

C.S. and F.S. performed the experiments. C.S. performed the data analysis. M.A. developed the kinetic simulation model. S.Z. and A.T.K. gave scientific and conceptual advice. S.Z. supervised the research project. All authors contributed to discussions and the manuscript.

Notes

The authors declare no competing financial interest.

Acknowledgements

Funded by the Deutsche Forschungsgemeinschaft (DFG, German Research Foundation) - 318063177.

References

(1) Fernández-Maestre, R.; Hill, H. H. Ion mobility spectrometry for the rapid analysis of over-the-counter drugs and beverages. *Int. J. Ion Mobil. Spec.* **2009**, *12*, 91–102.

(2) Zaknoun, H.; Binette, M.-J.; Tam, M. Analyzing fentanyl and fentanyl analogues by ion mobility spectrometry. *Int. J. Ion Mobil. Spec.* **2019**, *58*, 366.

(3) R.G. Ewing; D.A. Atkinson; G.A. Eiceman; G.J. Ewing. A critical review of ion mobility spectrometry for the detection of explosives and explosive related compounds. *Talanta* **2001**, *54*, 515–529.

(4) Tabrizchi, M.; Ilbeigi, V. Detection of explosives by positive corona discharge ion mobility spectrometry. *Journal of hazardous materials* **2010**, *176*, 692–696.

(5) Eiceman, G. A.; Stone, J. A. Peer Reviewed: Ion Mobility Spectrometers in National Defense. *Anal. Chem.* **2004**, *76*, 390A–397A.

(6) Mäkinen, M. A.; Anttalainen, O. A.; Sillanpää, Mika E T. Ion mobility spectrometry and its applications in detection of chemical warfare agents. *Anal. Chem.* **2010**, *82*, 9594–9600.
(7) Borsdorf, H.; Schelhorn, H.; Flachowsky, J.; Döring, H.-R.; Stach, J. Corona discharge ion mobility spectrometry of aliphatic and aromatic hydrocarbons. *Anal. Chim. Acta* **2000**, *403*, 235–242.
(8) Baumbach, J. I.; Sielemann, S.; Xie, Z.; Schmidt, H. Detection of the Gasoline Components Methyl tert -Butyl Ether, Benzene, Toluene, and m -Xylene Using Ion Mobility Spectrometers with a Radioactive and UV Ionization Source. *Anal. Chem.* **2003**, *75*, 1483–1490.
(9) Kirk, A. T.; Küddelsmann, M. J.; Bohnhorst, A.; Lippmann, M.; Zimmermann, S. Improving Ion Mobility Spectrometer Sensitivity through the Extended Field Switching Ion Shutter. *Anal. Chem.* **2020**, *92*, 4838-4847.
(10) Wissdorf, W.; Seifert, L.; Derpmann, V.; Klee, S.; Vautz, W.; Benter, T. Monte Carlo simulation of ion trajectories of reacting chemical systems: mobility of small water clusters in ion mobility spectrometry. *J. Am. Soc. Mass Spectrom.* **2013**, *24*, 632–641.
(11) Spanel, P.; Smith, D. Reactions of Hydrated Hydronium Ions and Hydrated Hydroxide Ions with Some Hydrocarbons and Oxygen-Bearing Organic Molecules. *J. Phys. Chem.* **1995**, *99*, 15551–15556.
(12) Bohme, D. K.; Mackay, G. I. Bridging the gap between the gas phase and solution: transition in the kinetics of nucleophilic displacement reactions. *J. Am. Chem. Soc.* **1981**, *103*, 978–979.
(13) Bohme, D. K.; Mackay, G. I.; Tanner, S. D. An experimental study of the gas-phase kinetics of reactions with hydrated hydronium(1+) ions(n = 1-3) at 298 K. *J. Am. Chem. Soc.* **1979**, *101*, 3724–3730.
(14) Langejürgen, J.; Allers, M.; Oermann, J.; Kirk, A. T.; Zimmermann, S. High kinetic energy ion mobility spectrometer: quantitative analysis of gas mixtures with ion mobility spectrometry. *Anal. Chem.* **2014**, *86*, 7023–7032.
(15) Wannier, G. H. Motion of Gaseous Ions in Strong Electric Fields. *Bell Syst. Tech. J.* **1953**, *32*, 170–254.
(16) Allers, M.; Kirk, A. T.; Eckermann, M.; Schaefer, C.; Erdogdu, D.; Wissdorf, W.; Benter, T.; Zimmermann, S. Positive Reactant Ion Formation in High Kinetic Energy Ion Mobility Spectrometry (HiKE-IMS). *J. Am. Soc. Mass Spectrom.* **2020**, *31*, 1291–1301.
(17) Allers, M.; Kirk, A. T.; Schaefer, C.; Schlottmann, F.; Zimmermann, S. Formation of positive product ions from substances with low proton affinity in High Kinetic Energy Ion Mobility Spectrometry (HiKE-IMS). *Rapid Communications in Mass Spectrometry* **2020**, e8998.
(18) Španěl, P.; Spesyvyi, A.; Smith, D. Electrostatic Switching and Selection of H3O+, NO+, and O2+• Reagent Ions for Selected Ion Flow-Drift Tube Mass Spectrometric Analyses of Air and Breath. *Anal. Chem.* **2019**, *91*, 5380–5388.
(19) Španěl, P.; Smith, D. Dissociation of H3O+, NO+ and O2+• reagent ions injected into nitrogen carrier gas in SIFT-MS and reactivity of the ion fragments. *Int. J. Mass Spectrom.* **2020**, 116438.
(20) Jordan, A.; Haidacher, S.; Hanel, G.; Hartungen, E.; Herbig, J.; Märk, L.; Schottkowsky, R.; Seehauser, H.; Sulzer, P.; Märk, T. D. An online ultra-high sensitivity Proton-transfer-reaction mass-spectrometer combined with switchable reagent ion capability (PTR+SRI−MS). *Int. J. Mass Spectrom.* **2009**, *286*, 32–38.
(21) Sulzer, P.; Agarwal, B.; Jürschik, S.; Lanza, M.; Jordan, A.; Hartungen, E.; Hanel, G.; Märk, L.; Märk, T. D.; González-Méndez, R.; Watts, P.; Mayhew, C. A. Applications of switching reagent ions in proton transfer reaction mass spectrometric instruments for the improved selectivity of explosive compounds. *Int. J. Mass Spectrom.* **2013**, *354-355*, 123–128.
(22) Allers, M.; Kirk, A. T.; Roßbitzky, N. von; Erdogdu, D.; Hillen, R.; Wissdorf, W.; Benter, T.; Zimmermann, S. Analyzing Positive Reactant Ions in High Kinetic Energy Ion Mobility Spectrometry (HiKE-IMS) by HiKE-IMS-MS. *J. Am. Soc. Mass Spectrom.* **2020**, *31*, 812-821.

(23) Langejürgen, J.; Allers, M.; Oermann, J.; Kirk, A. T.; Zimmermann, S. Quantitative detection of benzene in toluene- and xylene-rich atmospheres using high-kinetic-energy ion mobility spectrometry (IMS). *Anal. Chem.* **2014**, *86*, 11841–11846.
(24) Shahin, M. M. Mass-Spectrometric Studies of Corona Discharges in Air at Atmospheric Pressures. *J. Chem. Phys.* **1966**, *45*, 2600.
(25) Good, A. Ion–Molecule Reactions in Pure Nitrogen and Nitrogen Containing Traces of Water at Total Pressures 0.5–4 torr. Kinetics of Clustering Reactions Forming H+(H2O)n. *J. Chem. Phys.* **1970**, *52*, 212.
(26) Cunningham, A. J.; Payzant, J. D.; Kebarle, P. Kinetic study of the proton hydrate H+(H2O)n equilibriums in the gas phase. *J. Am. Chem. Soc.* **1972**, *94*, 7627–7632.
(27) Lau, Y. K.; Ikuta, S.; Kebarle, P. Thermodynamics and kinetics of the gas-phase reactions H3O+(H2O)n-1 + water = H3O+(H2O)n. *J. Am. Chem. Soc.* **1982**, *104*, 1462–1469.
(28) Gouw, J. de; Warneke, C.; Karl, T.; Eerdekens, G.; van der Veen, Carina; Fall, R. Sensitivity and specificity of atmospheric trace gas detection by proton-transfer-reaction mass spectrometry. *Int. J. Mass Spectrom.* **2003**, *223-224*, 365–382.
(29) Pavlik, M.; Skalny, J. D. Generation of [H3O]+.(H2O)n clusters by positive corona discharge in air. *Rapid Commun. Mass Spectrom.* **1997**, *11*, 1757–1766.
(30) Howard, C. J. Kinetics and Mechanism of the Formation of Water Cluster Ions from O[sub 2]+] and H2O. *J. Chem. Phys.* **1972**, *57*, 3491.
(31) Fehsenfeld, F. C.; Mosesman, M.; Ferguson, E. E. Ion—Molecule Reactions in an O 2 +–H 2 O System. *J. Chem. Phys.* **1971**, *55*, 2115–2120.
(32) Raksit, A. B. Reactions of O2+, O4+ and O2+·H2O ions with neutral molecules. *Int. J. Mass Spectrom. Ion Process.* **1986**, *69*, 45–65.
(33) French, M. A.; Hills, L. P.; Kebarle, P. Kinetics and Temperature Dependence of the Hydration of NO + in the Gas Phase. *Can. J. Chem.* **1973**, *51*, 456–461.
(34) Su, T.; Bowers, M. T. Ion-polar molecule collisions. Effect of molecular size on ion-polar molecule rate constants. *J. Am. Chem. Soc.* **1973**, *95*, 7609–7610.
(35) Ellis, A. M.; Mayhew, C. A. *Proton transfer reaction mass spectrometry: Principles and applications*; John Wiley & Sons, Ltd: Chichester, UK, 2014.
(36) Goebbert, D. J.; Wentold, P. G. Water dimer proton affinity from the kinetic method: dissociation energy of the water dimer. *Eur J Mass Spectrom (Chichester, Eng)* **2004**, *10*, 837–846.
(37) Cheng, H.-P. Water Clusters: Fascinating Hydrogen-Bonding Networks, Solvation Shell Structures, and Proton Motion. *J. Phys. Chem. A* **1998**, *102*, 6201–6204.
(38) Wróblewski, T.; Gazda, E.; Mechlińska-Drewko, J.; Karwasz, G. P. Swarm experiment on ionized water clusters. *Int. J. Mass Spectrom.* **2001**, *207*, 97–110.
(39) Kawai, Y.; Yamaguchi, S.; Okada, Y.; Takeuchi, K.; Yamauchi, Y.; Ozawa, S.; Nakai, H. Reactions of protonated water clusters H+(H2O)n (n=1–6) with dimethylsulfoxide in a guided ion beam apparatus. *Chemical Physics Letters* **2003**, *377*, 69–73.
(40) Eiceman, G. A.; Karpas, Z.; Hill, H. H. *Ion mobility spectrometry*, 3rd ed.; CRC Press: Boca Raton, 2013.
(41) Safaei, Z.; Willy, T. J.; Eiceman, G. A.; Stone, J. A.; Sillanpää, M. Quantitative response in ion mobility spectrometry with atmospheric pressure chemical ionization in positive polarity as a function of moisture and temperature. *Anal. Chim. Acta* **2019**, *1092*, 144–150.
(42) Sunner, J.; Nicol, G.; Kebarle, P. Factors determining relative sensitivity of analytes in positive mode atmospheric pressure ionization mass spectrometry **1988**, *60*, 1300–1307.
(43) Linstrom, P. *NIST Chemistry WebBook, NIST Standard Reference Database 69*, 1997.
(44) Spanel, P.; Smith, D. SIFT studies of the reactions of H3O+, NO+ and O2+ with a series of alcohols. *Int. J. Mass Spectrom. Ion Process.* **1997**, *167-168*, 375–388.

(45) Smith, D.; Wang, T.; Španěl, P. A SIFT study of the reactions of H2ONO+ ions with several types of organic molecules. *Int. J. Mass Spectrom.* **2003**, *230*, 1–9.
(46) Španěl, P.; Smith, D. Selected ion flow tube studies of the reactions of H3O+, NO+, and O2+ with several aromatic and aliphatic hydrocarbons. *Int. J. Mass Spectrom.* **1998**, *181*, 1–10.
(47) Midey, A. J.; Williams, S.; Arnold, S. T.; Viggiano, A. A. Reactions of H3O+(H2O)0,1 with Alkylbenzenes from 298 to 1200 K. *J. Phys. Chem. A* **2002**, *106*, 11726–11738.
(48) Williams, S.; Midey, A. J.; Arnold, S. T.; Morris, R. A.; Viggiano, A. A.; Chiu, Y.-H.; Levandier, D. J.; Dressler, R. A.; Berman, M. R. Electronic, Rovibrational, and Translational Energy Effects in Ion−Alkylbenzene Charge-Transfer Reactions †. *J. Phys. Chem. A* **2000**, *104*, 10336–10346.
(49) Arnold, S. T.; Williams, S.; Dotan, I.; Midey, A. J.; Morris, R. A.; Viggiano, A. A. Flow Tube Studies of Benzene Charge Transfer Reactions from 250 to 1400 K. *J. Phys. Chem. A* **1999**, *103*, 8421–8432.
(50) Kirk, A. T.; Grube, D.; Kobelt, T.; Wendt, C.; Zimmermann, S. A High Resolution High Kinetic Energy Ion Mobility Spectrometer Based on a Low-Discrimination Tristate Ion Shutter. *Anal. Chem.* **2018**, *90*, 5603-5611.
(51) Atkins, P. W.; Paula, J. de; Keeler, J. *Atkins' physical chemistry*, Eleventh edition; Oxford University Press: Oxford, New York, 2018.
(52) Kirk, A. T.; Kobelt, T.; Spehlbrink, H.; Zimmermann, S. A Simple Analytical Model for Predicting the Detectable Ion Current in Ion Mobility Spectrometry Using Corona Discharge Ionization Sources. *J. Am. Soc. Mass Spectrom.* **2018**, *29*, 1425–1430.
(53) Allers, M.; Kirk, A. T.; Schaefer, C.; Erdogdu, D.; Wissdorf, W.; Benter, T.; Zimmermann, S. Field dependent reduced ion mobilities of positive and negative ions in air and nitrogen in High Kinetic Energy Ion Mobility Spectrometry (HiKE-IMS). *J. Am. Soc. Mass Spectrom.* **2020**, Under review.
(54) Schlottmann, F.; Kirk, A. T.; Allers, M.; Bohnhorst, A.; Zimmermann, S. High Kinetic Energy Ion Mobility Spectrometry (HiKE-IMS) at 40 mbar. *J. Am. Soc. Mass Spectrom.* **2020**, *31*, 1536–1543.
(55) Lau, Y. K.; Nishizawa, K.; Tse, A.; Brown, R. S.; Kebarle, P. Protonation and site of protonation of anilines. Hydration and site of protonation after hydration. *J. Am. Chem. Soc.* **1981**, *103*, 6291–6295.
(56) Kolboe, S. Proton Affinity Calculations with High Level Methods. *Journal of chemical theory and computation* **2014**, *10*, 3123–3128.
(57) Johnson, R. D. *Computational Chemistry Comparison and Benchmark Database, NIST Standard Reference Database 101*, 2002.

For Table of Contents Use Only

Influence of Reduced Field Strength on Product Ion Formation in High Kinetic Energy Ion Mobility Spectrometry (HiKE-IMS)

Christoph Schaefer*, Maria Allers, Ansgar T. Kirk, Florian Schlottmann, Stefan Zimmermann